LIQUID-VAPOUR PHASE DIAGRAMS OF WATER IN NANOPORES

Confinement vs. surface effects

I. Brovchenko, A. Geiger, A. Oleinikova
Physikalische Chemie, Universitat Dortmund
44221 Dortmund, Germany

Abstract

Coexistence curves of water in nanopores were simulated in the Gibbs ensemble. Evolution of the coexistence curves with strength of the water-pore interaction and pore size is analysed. The surface effect is found to be the dominant factor, which determines the water phase diagrams in nanopores. The possible ranges of critical temperatures of liquid-vapour and layering transitions of water in pores are estimated. A new low-temperature surface transition is found in the pore with a model superhydrophobic wall.

1. Introduction

Phase diagrams of fluids in pores are strongly modified by a combination of the influence of the finite size of the system and surface effects, such as changes of the structure of the fluid due to interactions with the wall [1]. Moreover, surface phase transitions, such as layering, may split from the remaining liquid-vapour transition [2]. To understand the expected rich phase behaviour of fluids in pores, these effects have to be analysed for possible ranges of pore size, shape, fluid-wall and fluid-fluid interaction. Molecular simulations provide a realistic (although difficult) way for studying the phase behaviour of fluids. Two direct methods were applied for the simulation of coexistence curves of fluids in pores: Molecular Dynamics [3] and Gibbs ensemble Monte Carlo simulations [4]. Untill now only very few simulated coexistence curves of simple fluids in pores are available [5], prohibiting a systematic analysis.

The phase behaviour of water in pores is of special interest in view of its importance for understanding biological and industrial processes.

Localization of the regions of two-phase coexistence in the T - ϱ plane and knowledge of the densities of the coexisting phases is the basis for a correct simulation of the properties of water in pores. This is especially important for understanding the water properties in incompletely filled pores. (Another practically important situation is the equilibrium of water in a pore with an external bulk reservoir. See [6,7] and reference therein.)

We report a study of the coexistence line of water in nanopores with smooth surface, obtained by simulations in the Gibbs ensemble. The strength of the water-pore interaction varied from hydrophobic to hydrophilic. The evolution of the coexistence curve (critical temperature, shape of the coexistence curve, appearance of surface transitions) with varying water-pore interaction and pore size is analysed. Besides, a narrow cylindrical pore with a repulsive step near the pore wall was used to analyse the effect of a model superhydrophobic surface [8] on the coexistence curve of water.

2. Method

TIP4P water [9] in cylindrical and slit-like pores of 24 to 60 $\mathring{A}$ diameters (width) was simulated with periodic boundary conditions applied in one (cylindrical pores) and two (slit-like pores) dimensions. The water-pore interaction was simulated as Lennard-Jones (LJ) (9-3) potential, which depends on the distance between the oxygen atom and the pore surface only. The parameter σ of this potential was fixed at 2.5 $\mathring{A}$, whereas the parameter ϵ was varied to change the well-depth U = -0.39 ϵ from -0.39 kcal/mol to -4.62 kcal/mol. That approximately covers the range from hydrophobic to hydrophilic substrates. Gibbs ensemble Monte Carlo simulations [4] were used to obtain water phase coexistence. The two coexisting phases are represented in two simulation boxes. The water in both boxes is kept at the same temperature and the equality of pressure is provided by simultaneous changes of the box volumes. The total number N of molecules in the two boxes is fixed during the simulation (N ranges from 400 to 3000 depending on pore size and shape). The distribution of molecules between the two boxes changes in the course of a simulation due to the molecular transfers, which provide equality of the chemical potential in the two coexisting phases.

Low efficiency of molecular insertion (deletion) in (from) the dense phase, especially at low temperatures, is the main factor, which limits the applicability of the Gibbs ensemble simulation. The efficiency of molecule deletions was improved by a biased choice of more loosely bound molecules [6]. The efficiency of molecule insertions was improved

by early rejection of the new configuration if at least one of the interatomic distances between the inserted molecule and other molecules is shorter than some reference value [10]. The acceptance probability was corrected by a factor, equal to the probability to find at random a molecule with energy higher than the chosen reference energy (in the case of deletion) or with shortest interatomic distances, exceeding the chosen reference distances (in the case of insertion). These techniques allow to extended the simulation of the liquid-vapour coexistence curve of bulk water in the supercooled region down to 200 K [10] (see Fig1.a).

The water density in the pore was calculated by assuming that a shell of width $\sigma/2$ near the pore wall is inaccessible to water.

3. Results

3.1 Coexistence curves of water in hydrophobic and hydrophilic pores

The obtained coexistence curves of water in cylindrical pores with radius $R_C = 12$ Å are presented in Fig.1. The liquid-vapour critical temperature in the pore T_P strongly decreases with respect to the bulk value ($T_{3D} \approx 579$ K, [10]) with strengthening of the water-pore interaction (Fig.1, b-d): $T_P \approx 0.93T_{3D}$ at U = -0.39 kcal/mol, $T_P \approx 0.90T_{3D}$ at U = -1.93 kcal/mol, $T_P \approx 0.80T_{3D}$ at U = -3.08 kcal/mol. The shape of the liquid-vapour coexistence curve also strongly depends on U. Strengthening water-pore interaction makes the top of the coexistence curve more flat.

When the parameter U achieves -3.85 kcal/mol, the coexistence curve splits into two regions (Fig.1.e): coexistence between vapour and two water layers, adsorbed on the pore wall (solid circles) and liquid-vapour coexistence in the inner part of the pore (open circles). In the low temperature region of Fig.1.e only liquid-vapour coexistence is observed. This suggests the existence of a triple point near $T \approx 250$ K and $\varrho \approx 0.8$ g*cm^{-3}.

Further strengthening of the water-pore interaction (U = -4.62 kcal/mol) results in the appearance of three kinds of phase coexistence in the pore (Fig.1.f): 1st layering transition, i.e. liquid-vapour coexistence in the first outer layer (low density region); 2nd layering transition (open circles) and liquid-vapour coexistence in the inner part of the pore. The same three regions of two-phase coexistence are observed also for slit-like pores.

The critical temperature of the 1st layering transition T_{1L} is not very sensitive to pore size and shape and varies in the range 0.68 to $0.70T_{3D}$. The critical temperature of the 2nd layering transition T_{2L} is always

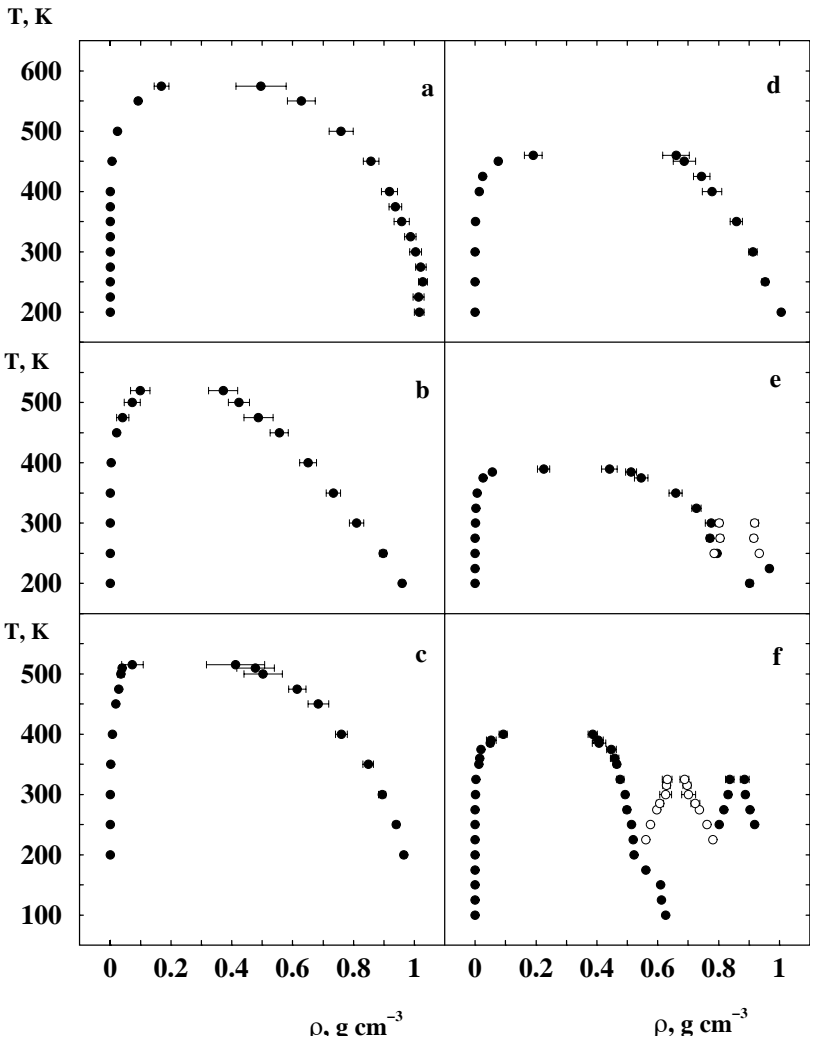

Figure 1. Coexistence curves of the bulk water (a) and water confined in cylindrical pores with radius R_C = 12 Å. (b) U = -0.39 kcal/mol. (c) U = -1.93 kcal/mol. (d) U = -3.08 kcal/mol. (e) U = -3.85 kcal/mol. (f) U = -4.62 kcal/mol.

lower than T_{1L}. With increasing pore size the 2nd layering transition disappears (for cylindrical pores between R_C = 15 Å and R_C = 20 Å).

The density interval of the two-phase coexistence, corresponding to the 1st layering transition, is proportional to the ratio of the volume of the first water layer to the total pore volume. This ratio decreases

with increasing pore size, going to zero at $R_C \to \infty$. In parallel, the density interval, corresponding to the liquid-vapour coexistence in the inner part of the pore, extends and becomes the most typical two-phase coexistence in larger hydrophilic pores (Fig.2, bottom panel).

The critical temperature T_I of the liquid-vapour phase transition of this "inner" water confined within two water layers in hydrophilic pores (U = -4.62 kcal/mol), varies strongly with changes of the pore size. In cylindrical pores T_I changes from $0.59T_{3D}$ at $R_C = 12$ Å to $0.80T_{3D}$ at $R_C = 20$ Å and to $\geq 0.96T_{3D}$ at $R_C = 25$ Å. Contrary to this, in hydrophobic pores (U = -0.39 kcal/mol) the liquid-vapour critical temperature T_P is surprisingly insensitive to variations of the pore size in the considered range. When the radius R_C of hydrophobic cylindrical pores changes from 12 Å to 20 Å, T_P varies from 0.92 to $0.94T_{3D}$, which is not distinguishable within the accuracy of the simulation method.

3.2 Structural properties of water in pores

Structural properties of water in pores were calculated on the basis of the obtained water densities along the coexistence curves. The density distributions of oxygen and hydrogen atoms in the liquid phase along the pore radius are shown in Fig.3 for pores with different strengths of water-pore interaction. Strong density variations, indicating the appearance of two pronounced water layers near the pore wall, are observed in all considered pores, except the hydrophobic one (Fig3.e). Despite an orientationaly independent interaction of the water molecules with the wall, strengthening water-pore interaction causes strong orientational ordering of water molecules near the hydrophilic wall. This is reflected in specific maxima of the hydrogen atom density in between the two water layers.

The specific structure of the first outer layer of water in hydrophilic pores is shown in Fig. 4. Hydrogen-bonded quasi-planar water polygons dominate at low temperatures, whereas at higher temperatures there are hydrogen-bonded chains of water molecules. This structure reflects also in the oxygen-oxygen pair correlation functions $g_{OO}(r)$ (Fig.5). A pronounced maximum at 5.5 Å of $g_{OO}(r)$ in the first layer, that corresponds to the doubling of the first maximum position, is observed for all pores, excluding the hydrophobic one only. Decrease of the temperature improves the tetrahedral water structure, this is indicated by the increase of the tetrahedral maximum at 4.40 Å, whereas the maximum of $g_{OO}(r)$ at 5.5 Å persists in a wider temperature range than the tetrahedral maximum does.

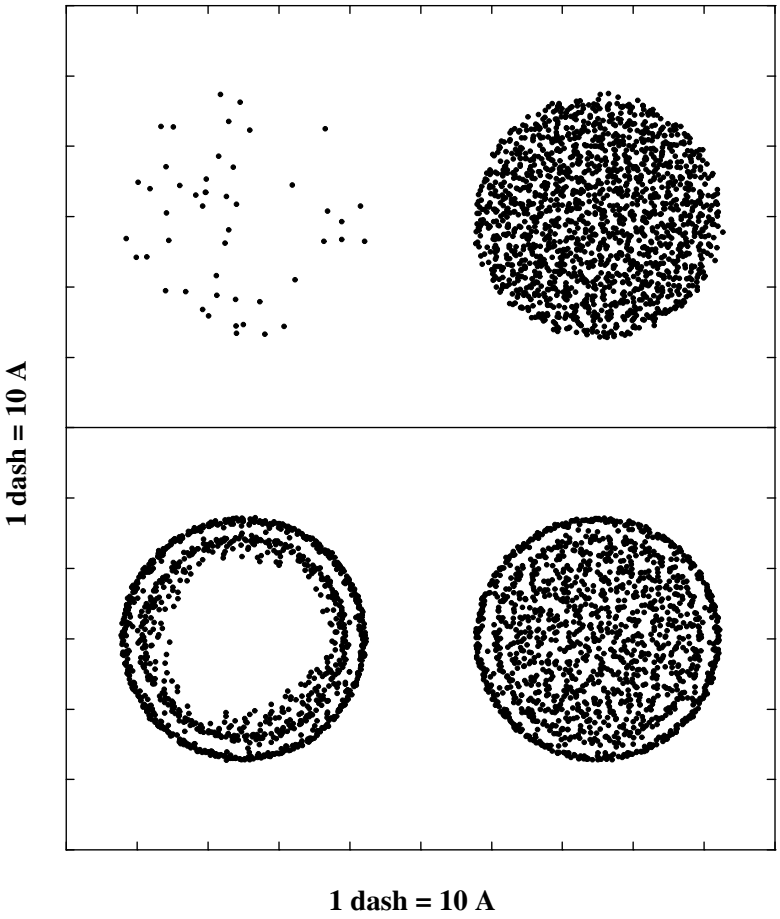

Figure 2. Arrangement of oxygen atoms in the typical coexisting phases of water in cylindrical hydrophobic (top panel) and hydrophilic (bottom panel) pores. R_C = 20 $\AA$. T = 300 K. View along the pore axis.

3.3 Coexistence curve of water in a superhydrophobic pore

We have simulated the coexistence curve of water in a cylindrical pore with R_C = 10 $\AA$ and a wall potential which should model a superhydrophobic surface. A repulsive step of 0.2 kcal/mol height and 3 $\AA$ width (between 7 and 10 $\AA$ from the pore axis) was added to a hard wall at 10 $\AA$ from the pore axis (see Fig.7, lower panel), modelling in a simplified

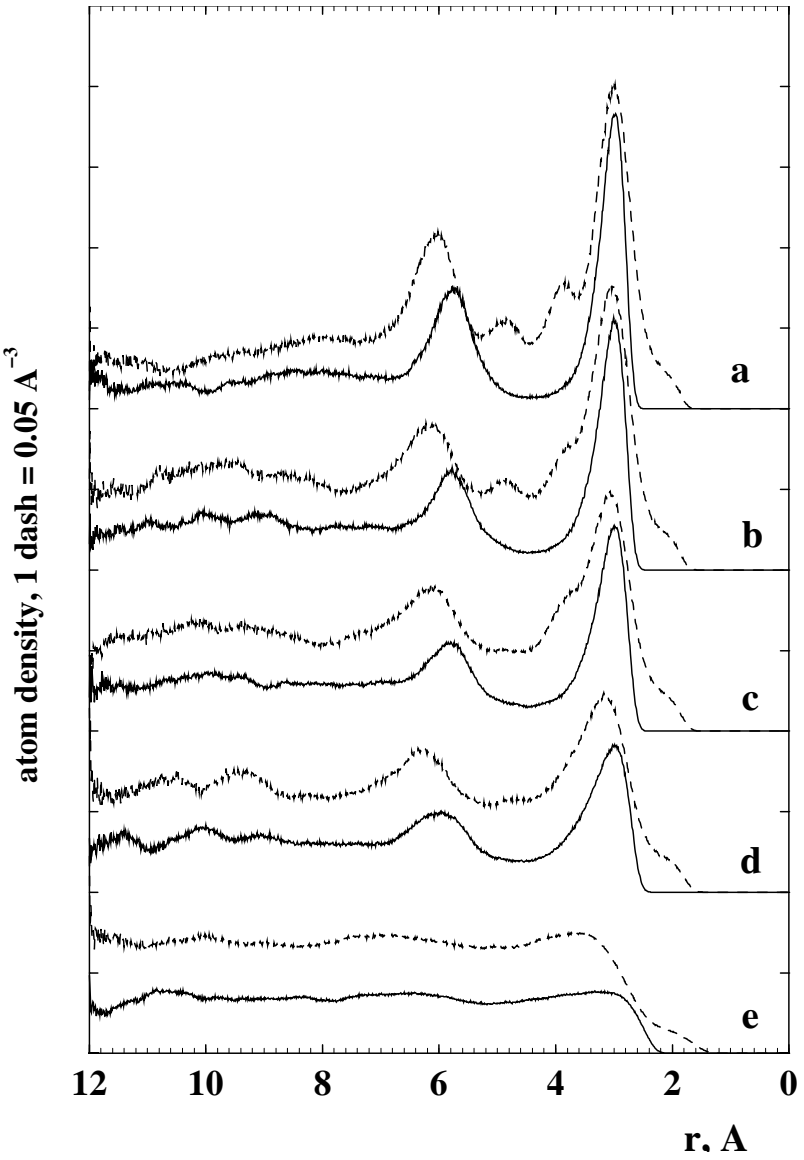

Figure 3. Oxygen (solid lines) and hydrogen (dashed lines) atom density distribution of water along the radius of cylindrical pores with R_C = 12 *Å*. Liquid branch of the coexistence curve at T = 300 K. a) U = -4.62 kcal/mol; b) U = -3.85 kcal/mol; c) U = -3.08 kcal/mol; d) U = -1.93 kcal/mol; e) U = -0.39 kcal/mol.

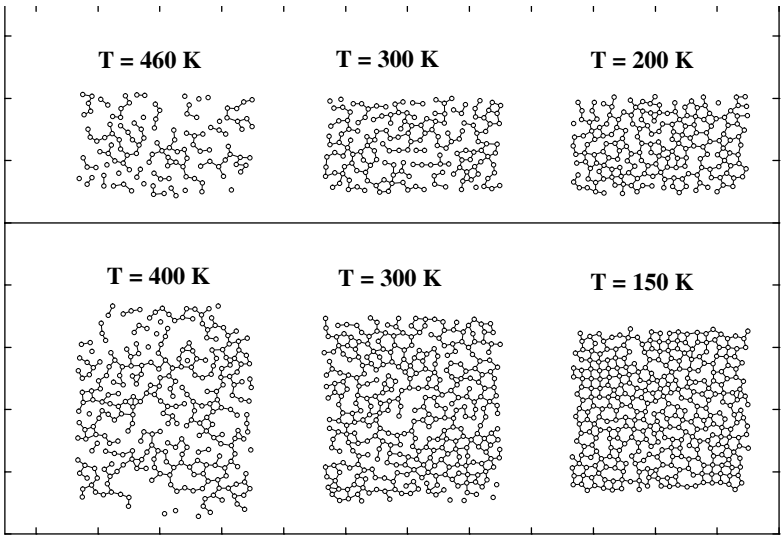

Figure 4. Quasi-planar water-water hydrogen bond patterns in the first outer layer in cylindrical pores with R_C = 12 Å. Lower panel: single water layer in the pore with U = -4.62 kcal/mol (see Fig.1.f). Upper panel: first outer layer in the pore with U = -3.08 kcal/mol (see Fig1.d). 1 dash = 20 Å.

way the interaction of water with a hydrophobic surface of appropriate roughness to hinder the approach of water [8].

The obtained coexistence curve is shown in Fig. 6. A pronounced density maximum of the liquid branch of the liquid-vapour coexistence curve at the temperature about 290 K is clearly seen. In addition, a new low-temperature two-phase region is observed at high densities (Fig.6, open circles). The critical point of this transition is located around 240 K. The corresponding coexisting phases differ mainly by the densities in the surface layer (see Fig.7, upper panel). An accurate analysis of the structural properties of water in this pore is complicated by its narrowness and cylindrical shape.

4. Discussion

The simulated coexistence curves of water in pores show two-phase states of confined water in wide intervals of temperature and density. This indicates the necessity to take into account typical two-phase states of water in pores both in computer simulations and in the analysis of ex-

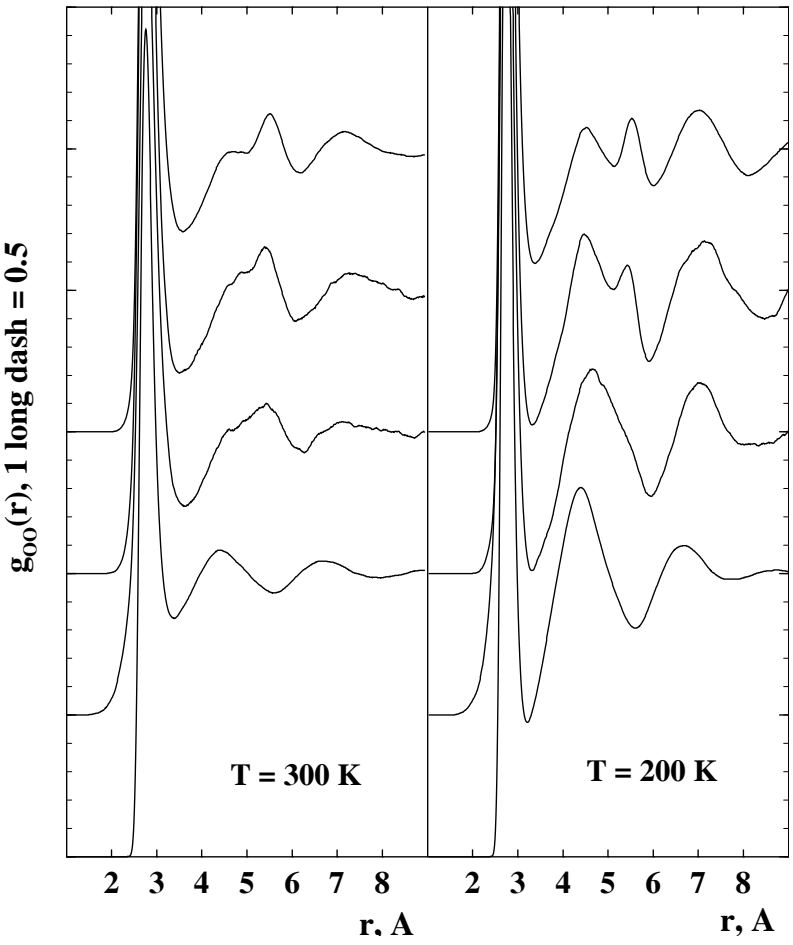

Figure 5. "In-layer" pair correlation functions g_{OO}(r) of water in the first layer of the cylindrical pores with R_C = 12 Å and g_{OO}(r) of the bulk water. From top to bottom: U = -4.62 kcal/mol (single water layer), U = -3.08 kcal/mol, U = -1.93 kcal/mol, bulk water.

perimental results. Neglecting the possibility of water phase separation in pores may result in the simulation of thermodynamically unstable states.

By varying the strength of water-pore interaction in a wide range we can trace the evolution of the coexistence curve of water in pores in detail. In hydrophobic pores with a surface close to a hard wall the liquid-vapour coexistence curve is narrower than in the bulk. To charac-

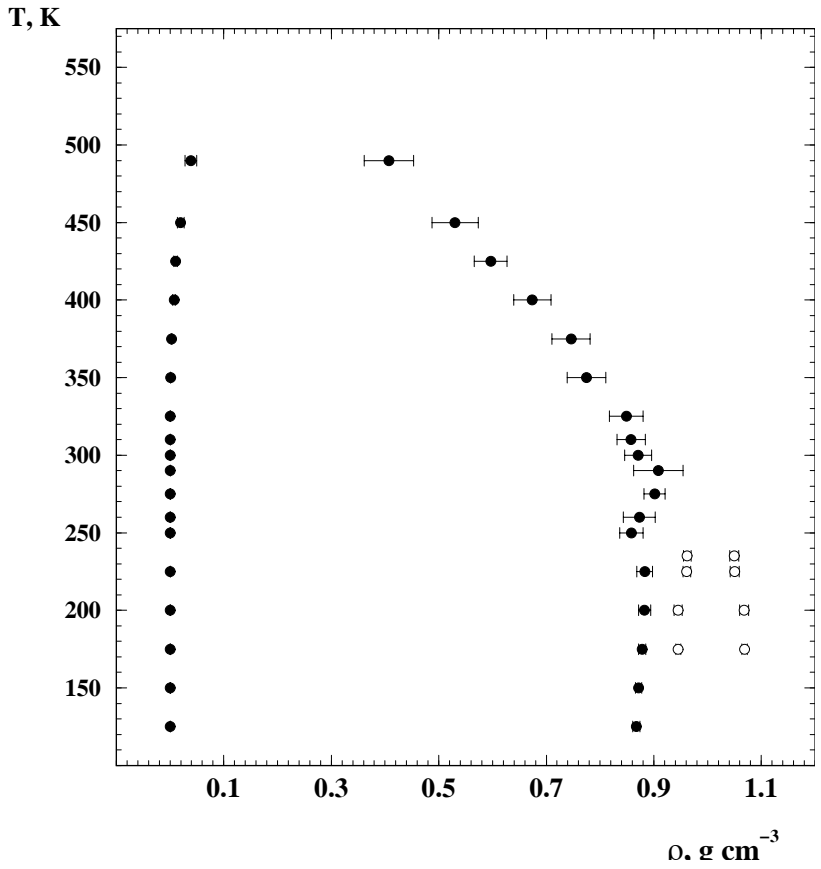

Figure 6. Coexistence curve of water in a superhydrophobic cylindrical pore (R_C = 10 Å) with a repulsive step near the pore wall.

terize the evolution of the shape of the coexistence curve quantitatively we use the effective exponent β_{eff} that describes the temperature dependence of the order parameter $\Delta\varrho = (\varrho_1 - \varrho_2)/2$ in a wide temperature range via $\Delta\varrho \sim (T_C - T)^{\beta_{eff}}$, where ϱ_1 and ϱ_2 are average or local densities of the coexisting phases. An analysis of the local order parameter along the pore radius shows [10], that water in the surface layer of hydrophobic pore disorders with temperature more strongly than the water in the interior of the pore, obeying a power law with an effective critical exponent β_{eff} value close to the surface critical exponent $\beta_1 \approx 0.8$ of a semi-infinite Ising magnet at an ordinary transition [11]. As a result the effective exponent β_{eff} of the pore coexistence curve, determined for

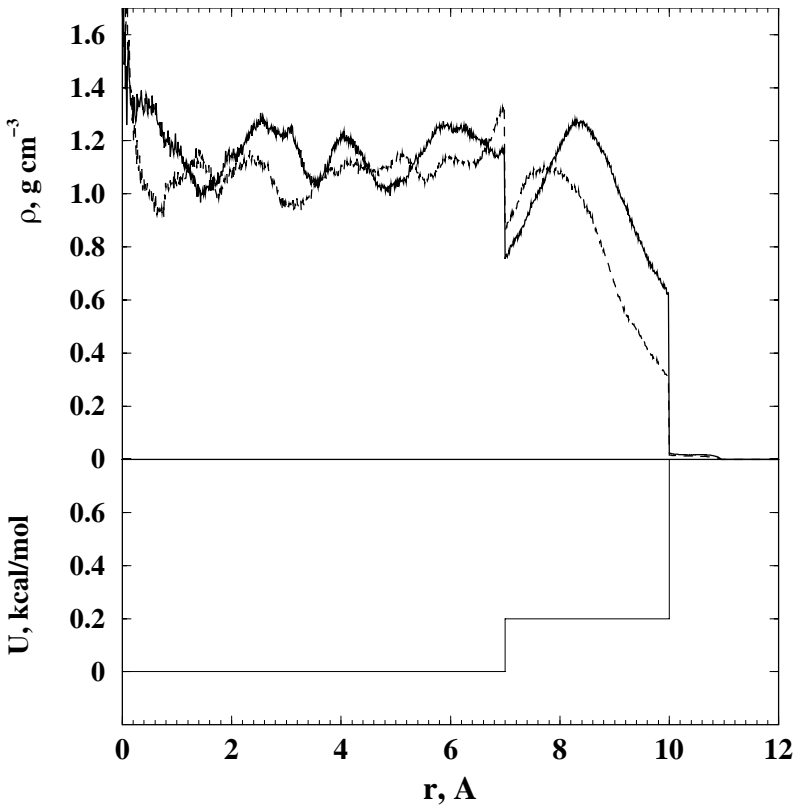

Figure 7. Water density distributions along the pore radius in two low-temperature coexisting phases (see Fig. 6, open circles). Superhydrophobic cylindrical pore, R_C = 10 Å, T = 200 K.

the average densities, essentially exceeds the 3D-Ising value. In particular, the apparent "mean-field behaviour" with the exponent $\beta_{eff} \approx 0.5$ observed experimentally [12,13] may be attributed to the surface effect discussed above. A normal (with non-zero surface field) and not ordinary (with zero surface field) transition is expected for the asymptotic critical behaviour of fluids near boundaries [14]. But in the limit of a weak surface field, fluids may show features of an ordinary transition at temperatures not too close to the critical temperature [15].

The critical temperature T_P in hydrophobic pores is found to be slightly below the bulk value T_{3D} ($T_P = 0.93T_{3D}$), and insensitive to changes of the pore size in the considered range, in apparent disagreement with theoretical expectations. This result may be connected with a

strong distortion of the shape of the coexistence curve due to the specific critical behaviour of the surface layer in hydrophobic pores.

Strengthening water-pore interaction increases the oscillations of the water density normal to the pore wall (Fig.3). Due to this layered structure, the system gets feature of two-dimensionality [16]. This results in a decrease of the value of the effective exponent β_{eff} towards the 2D Ising value and a flattening of the coexistence curve. The value β_{eff} in the cylindrical pores with $R_C = 12$ Å decreases from $\beta_{eff} = 0.46$ at U = -0.39 kcal/mol to $\beta_{eff} = 0.16$ at U = -3.08 kcal/mol. In parallel the shift ΔT_P of the pore critical temperature T_P changes from $\Delta T_P = 0.07 T_{3D}$ to $\Delta T_P = 0.20 T_{3D}$, respectively. This covers approximately the interval of possible shifts of the liquid-vapour critical temperature due to the variation of the strength of the water-pore interaction, as far as it is limited from below by the hard wall interaction and from above by the appearance of the layering transition. The obtained ratio of the maximal and minimal ΔT_P of about 2.9 is comparable with the theoretical predictions [17].

A layering transition with critical temperature $T_{1L} = 0.69 T_{3D}$ separates from the liquid-vapour transition when the parameter U of the water-pore potential gets close to the typical energy of pair interaction between water molecules (-4 to -5 kcal/mol). In order to clarify the effect of water-substrate interaction on the critical temperature of the layering transition we simulated the coexistence curve of water at a substrate with quasi-infinite attraction. This system was modelled by placing all water oxygens in one plane. Such quasi-2D-water shows a critical temperature $T_{2D} \approx 0.57 T_{3D}$, a ratio T_{2D}/T_{3D} which is essentially higher than for LJ fluids. So, the critical temperature of the water layering transition at a smooth surface may vary in the interval from $0.69 T_{3D}$ to $0.57 T_{3D}$.

The existence of a triple point, where vapour, liquid and surface layers coexist (Fig. 1.e) indicates the possibility of an additional phase transition, caused by the destabilization of the surface layers with respect to the vapour or liquid phase (depending on the average water density in the pore) below the triple point. This agrees with the recent observation of an additional low-temperature phase transition in pores, incompletely filled with water [18].

In hydrophilic pores the liquid-vapour phase transition of the "inner" water takes place in a cavity with a wall consisting of two highly ordered water layers (see Fig.2, lower panel). In this case the liquid-vapour pore critical temperature T_I proves to be highly sensitive to a variation of the pore size. T_I varies from $0.59 T_{3D}$ to $\geq 0.96 T_{3D}$, when the radius of the cylindrical pores changes from $R_C = 12$ Å to $R_C = 25$ Å, in qualitative

agreement with theoretical predictions for the finite-size effect [17]. This may be attributed to a significant reduction of the density oscillations of the "inner" water due to the specific wall, formed by two water layers.

The water molecules in the first outer layer in hydrophilic pores show a specific arrangement with an appearance of hydrogen bonded chains and polygons (Fig.4). This causes the appearance of an additional pair correlation of oxygens atoms at 5.5 $\mathring{A}$ (Fig.5).

In the model superhydrophobic pore with a repulsive step near the pore wall an additional low-temperature liquid-liquid coexistence was found (Fig.6). This phase transition may be the analogue of the layering surface transition near a hydrophilic wall and (or) may be caused by water polymorphism at low temperatures (note, that the critical temperature of this transition T $\approx$ 240 K is close to the expected liquid-liquid critical point of bulk water [19,20]). Simulations with larger pores with superhydrophobic surface are necessary in order to clarify the origin of this transition.

5. Conclusions

Coexistence curves of water in nanopores with smooth surface were simulated for a wide range of water-pore interaction. Strong changes of the pore critical temperature and the shape of the coexistence curve are found. The range of the possible variations of the critical temperatures of the liquid-vapour and layering transitions are estimated. New low-temperature phase transitions are found in a superhydrophobic pore.

The presented results show that the surface effect is the dominant factor, which determines the rich phase behaviour of water in nanopores. Analysis of the surface critical behaviour of fluids in the framework of the existing theory of boundary critical phenomena [14] is difficult because of the strong variation of density and intermolecular interaction near the surface. The shift of the critical parameters of the fluid in the pore makes this analysis even more complicated. Extended computer simulations of the fluid phase behaviour in pores allow to clarify these problems.

Acknowledgments

This work was supported by Ministerium fur Schule und Weiterbildung, Wissenschaft und Forschung des Landes Nordrhein-Westfalen.

References

[1] M. E. Fisher and H. Nakanishi, J. Chem. Phys. **75**, 5857 (1981).

[2] R. Evans, J. Phys. : Condens. Matter. **2**, 8989 (1990).

[3] G. S. Heffelfinger, F. Van Swol and K. E. Gubbins, Mol. Phys. **61**, 1381 (1987).

[4] A. Z. Panagiotopoulos, Mol. Phys. **62**, 701 (1987).

[5] L. D. Gelb, K. E. Gubbins, R. Radhakrishnan and M. Sliwinska-Bartkowiak, Rep. Prog. Phys. **62**, 1573 (1999).

[6] I. Brovchenko, D. Paschek and A. Geiger, J. Chem. Phys. **113**, 5026 (2000).

[7] I. Brovchenko, A. Geiger and D. Paschek, Fluid Phase Equilibria (2001).

[8] A. Nakajima. K. Hashimoto and T. Watanabe, Monatshefte fur Chemie **132**, 31 (2001).

[9] W. L. Jorgensen, J. Chandrasekhar, J. D. Madura, R. W. Impey and M. L. Klein, J. Chem. Phys. **79**, 926 (1983).

[10] I. Brovchenko, A. Geiger and A. Oleinikova, Phys. Chem. Chem. Phys. **3**, 1567 (2001).

[11] K. Binder, in *Phase Transitions and Critical Phenomena*, ed. by C. Domb and J. L. Lebowitz (Academic, London) 8 (1983) 1.

[12] M. Thommes and G. H. Findenegg, Langmuir **10**, 4270 (1994).

[13] L. D. Gelb, M. Sliwinska-Bartkowiak and K. E. Gubbins, Fundamentals of Adsorption **6**, 497 (1999).

[14] H. W. Diehl, Int. J. Mod. Phys. **B11**, 3503 (1997).

[15] W. Fenzl, Europhys. Lett. **24**, 557 (1993).

[16] M. E. Fisher, J. Vac. Sci. Technol. **10**, 665 (1973).

[17] H. Nakanishi and M. E. Fisher, J. Chem. Phys. **78**, 3279 (1983).

[18] A. Schreiber, I. Ketelsen and G. H. Findenegg, Phys. Chem. Chem. Phys. **3**, 1185 (2001).

[19] H. Tanaka, Nature **380**, 328 (1996).

[20] F. Sciortino, P. H. Poole, U. Essmann and H. E. Stanley, Phys. Rev. E **55**, 727 (1997).